

Comparison of different capillary bridge models for application in the discrete element method

Anton Gladkyy* and Rüdiger Schwarze*

* Institute of Mechanics and Fluid Dynamics, TU Bergakademie Freiberg,
Lampadiusstr. 4, 09596 Freiberg, Germany.

September 15, 2014

Weakly wetted granular material is the subject of many studies. Several formulations were proposed to calculate the capillary forces between wet particles. In this paper some of such models have been implemented in a DEM-framework, and simulation results were compared to experimental measurements. Also, the influence of capillary model type on macro parameters like local shear viscosity and cohesive parameters of sheared material have been investigated through the simulation of spherical beads using a DEM-model of a split-bottom shear-cell.

It was concluded that the water content, simulated with the help of capillary bridge models, changes the macro-properties of the simulated granular material. Different capillary bridge models do not influence the macroscopic results visibly.

1. Introduction

Wet granular materials play an important role in geology and many technical applications, e.g. construction, pharmaceuticals, civil engineering, etc. Here, liquid or capillary bridges are present between the grains, which produce inter-grain forces on the micro-scale level and drastically modify the mechanical properties of the granular media on the macro-scale levels (e.g. slopes can be much larger than 45 degrees for banked up wet bulk material) [6, 5, 14].

Such inter-grain capillary forces have been the subject of many investigations within the last decades, see e.g. [9, 5, 8] for an overview. Modern instruments allow one to measure micro- and even nano-scale force values between individual particles very precisely. Based on this experimental information, capillary bridge models (CBMs) for capillary

force calculations can be deduced, as described e.g. in [7]. Some recent studies in this direction have been done for instance by Willett et al. [27] and Rabinovich et al. [18].

These CBMs can be implemented in particle-based simulation methods, for example on the base of the Discrete Element Method (DEM), in order to model the effects of individual capillary bridges between particles. Using a CBM it is possible to simulate the behavior of wetted bulk material and to predict its macro-parameters. This is important for simulations of processes like agglomeration, adhesion, crystallization and others [22, 20, 11].

In this paper, we investigate four different CBMs, which have been frequently used to model capillary bridge forces in DEM simulations. Firstly, the CBM formulations and their implementations in an open-source DEM software package are summarized. Then, the quality of the CBM for the description of individual capillary bridges in the pendular regime (where the capillary bridges exist individually) is tested by comparison of experimental and numerical data. Finally, every CBM is analyzed in simulations of weakly wetted bulk material shear flows by cross-comparison of results from the different CBMs. Here, the bridges are again in pendular state.

2. Employed capillary bridge models

Zhu et al. [28] discuss in their review the main features of CBMs for the calculation of capillary forces. CBMs for application in DEM simulations should consist of easy to implement explicit functions of liquid bridge volume and the particle separa-

ration distance. Additionally, the shape of the liquid bridge must be approximated in order to calculate the capillary force.

The total capillary attractive force between two particles is caused by a surface tension component and hydrostatic pressure in the bulk [10].

Two different methods can be adopted: in the neck (or “gorge”) method the force is estimated at the neck of the bridge. In contrast, in the contact (or boundary) method, the force is evaluated at the liquid bridge solid contact region. It has been demonstrated that both methods provide relatively precise predictions of capillary forces [28].

Some recent approaches with explicit CBM functions have been proposed by Weigert and Ripperger [26] (contact method), Willett et al. [27] (neck method), Rabinovich et al. [18] (neck method) and Soulie et al. [25] (neck method). Lambert et al. [8] give a corrected version of Rabinovich’s CBM. Several of these CBMs have already been successfully used in DEM simulations of weakly wetted granular material [20, 3, 4, 13, 24]. A comparison of CBMs from Soulie and Rabinovich (with Lambert’s correction) has already been given in [3]. Therefore, we will compare all stated CBMs except Soulie’s in order to identify (i) differences between CBM based on the contact and the neck method and (ii) differences between CBMs based on the same method (neck) but with different formulations.

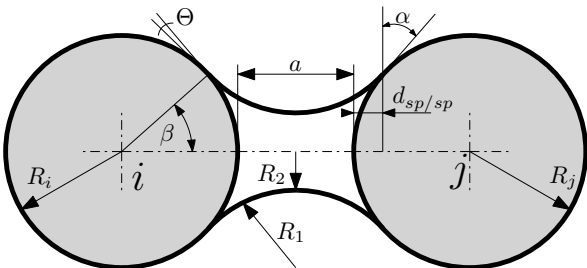


Figure 1: Pendular liquid bridge between two spherical particles. See the text for the description of the indicated parameters.

In our study, we apply four different CBMs, which have been proposed in chronological order by Weigert and Ripperger [26], Willett et al. [27] and Rabinovich et al. [18]) for the capillary force F_{cap} between particles i and j with radii R_i and R_j . In these models, an effective radius R of the particle pair (which is based on the Derjaguin approximation) is calculated as a harmonic mean of 2 different radii.

$$R = \frac{2R_i R_j}{R_i + R_j} \quad (1)$$

Willett et al. [27] have demonstrated that the

Derjaguin approximation works in a reasonable way for separation distances a excluding close-contact ($a \approx 0$) and near rupture distance ($a \approx a_{crit}$). Some limitations of this approach have been discussed by Rabinovich et al. [18].

As constant input parameters, we prescribe the liquid bridge volume $V = V_{bridge}$, the contact angle θ of the liquid-gas interface at the particle surface, and the liquid surface tension γ . In all four CBMs, the distance a between the surfaces of the two particles i, j is the main model variable (Fig. 1). We assume that F_{cap} (capillary force) is acting only after a mechanical contact between i and j . F_{cap} is acting as long as $a < a_{crit}$. The critical distance (rupture distance of the liquid bridge) a_{crit} between two particles is calculated according to Willett et al. [27]:

$$a_{crit}^* = \left(1 + \frac{\theta}{2}\right) \cdot \left(V^{*1/3} + \frac{V^{*2/3}}{10}\right) \quad (2)$$

Where $a_{crit}^* = a_{crit}/R$ and $V^* = V/R^3$ are the dimensionless critical distance and bridge volume accordingly.

All formulations, which are given below, have been implemented in the open-source DEM software Yade [29] in combination with a linear viscoelastic model for normal contacts [19]:

$$\begin{aligned} F_{norm} &= -k_n \delta_n - c_n \frac{d\delta_n}{dt} \\ F_{tan} &= -k_t \delta_t - c_t \frac{d\delta_t}{dt} \end{aligned} \quad (3)$$

Here, spring and damping parameters k_n, k_t, c_n and c_t are calculated as a function of restitution coefficients in normal and tangential directions e_n and e_t , contact duration time t_c and mass of particles, see [16] for details. The leapfrog algorithm is used for the integration of motion. Our model implementation is in line with the description given in [19].

The total interaction force acting on particle during the normal contact is the sum of normal and tangential forces Eq. (4). Coulomb’s friction law $|F_{tan}| \leq \mu_C F_{norm}$ as well as preventing undesirable attractive forces when $d\delta_n/dt > 0$ were considered in implementation [23]. Rolling resistance is neglected. The capillary force \vec{F}_{cap} is acting along the line connecting the centers of particles j and i .

$$\vec{F} = \begin{cases} \vec{F}_{norm} + \vec{F}_{tan}, & \delta_n < 0 \\ \vec{F}_{cap}, & \delta_n > 0 \end{cases} \quad (4)$$

We are neglecting effects of capillary forces during mechanical contact because we are not aware of a proved model for that case. Because the capillary forces are in order of magnitude much smaller

than the mechanical ones, we do not expect a large influence from this simplification.

2.1. Weigert's model

In the CBM of Weigert and Ripperger [26], empirical equations are employed in order to calculate V and the half-filling angle β from the bulk liquid saturation. These parameters are needed to calculate F_{cap} :

$$F_{cap} = \underbrace{\frac{\pi}{4}(2R)^2 \sin^2 \beta \cdot p_k}_{F_p} + \underbrace{\gamma \pi 2R \sin \beta \sin(\beta + \theta)}_{F_\gamma} \quad (5)$$

where the first term F_p is the hydrostatic pressure component and the second one F_γ is the liquid surface tension contribution. Both force components are evaluated at the particle surface. Main geometrical parameters of the liquid bridge are showed in figure 1.

Equations for all other parameters are presented in the appendix. The sequence of equations in implementation is the following: Eq. (A3), Eq. (A4), Eq. (A2), Eq. (A6), Eq. (A7), Eq. (A5), Eq. (5).

2.2. Willett's full model

Willett et al. [27] proposed the following CBM, which is based on combined experimental and numerical results with numerical data from integration of the Laplace-Young equation. The main model variable is the scaled, dimensionless half-separation distance S^+ :

$$S^+ = \frac{a}{2\sqrt{V/R}} \quad (6)$$

F_{cap} is calculated from:

$$F_{cap} = 2\pi R\gamma \exp(f_1 - f_2 \exp(f_3 \ln S^+ + f_4 \ln^2 S^+)) \quad (7)$$

The definitions of the coefficients $f_{1..4}$ are presented in the appendix and were derived by curve-fitting to the numerical solution. The sequence of equations in implementation is the following: Eq. (B1), Eq. (B2), Eq. (B3), Eq. (B4), Eq. (6), Eq. (7).

2.3. Willett's reduced model

Willett et al. [27] also give a less complex CBM for equal-sized particles $R_i = R_j = R$. The following equation provides a closed approximation of F_{cap} between equal-sized spheres:

$$F_{cap} = \frac{2\pi R\gamma \cos \theta}{1 + 2.1(S^+) + 10(S^+)^2} \quad (8)$$

The sequence of equations in implementation is the following: Eq. (6), Eq. (8).

Willett et al. [27] noticed that both proposed formulations are valid for $\theta < 50^\circ$ and $V^* < 0.1$.

2.4. Rabinovich's model

Rabinovich et al. [18] give the following CBM, which is based on combined experimental and numerical analysis as well. First of all, the "embracing angle" α for the case sphere-sphere is evaluated (see Fig. 1):

$$\alpha = \sqrt{\frac{a}{R} \cdot \left(-1 + \sqrt{1 + \frac{2V}{\pi R a^2}} \right)} \quad (9)$$

Then the immersion distance $d_{sp/sp}$ must be found:

$$d_{sp/sp} = \frac{a}{2} \cdot \left[-1 + \sqrt{1 + \frac{2V}{\pi R a^2}} \right] \quad (10)$$

Finally, F_{cap} is predicted with:

$$F_{cap} = -\frac{2\pi R\gamma \cos \theta}{1 + [a/2d_{sp/sp}]} - 2\pi\gamma R \sin \alpha \sin(\theta + \alpha) \quad (11)$$

Later, Lambert et al. [8] identified an error in the deduction of the model and showed that the second term of Eq. (11) is redundant. Therefore, we employ Rabinovich's model with Lambert's correction. F_{cap} is predicted with:

$$F_{cap} = -\frac{2\pi R\gamma \cos \theta}{1 + [a/2d_{sp/sp}]} \quad (12)$$

The sequence of equations in implementation is the following: Eq. (9), Eq. (10), Eq. (12).

3. Validation of capillary bridge model implementations

Here, we observe outputs (forces) of different CBMs during the DEM pendular simulation of a pair of particles with a single liquid bridge. The setup of the simulations corresponds to the experiments that are presented in Willett et al. [27] for micro-scale and in Rabinovich et al. [18] for nano-scale experiments.

Willett et al. [27] employed for the experiments precision synthetic sapphire spheres of radii 2.381, 1.588 and 1.191 mm. In their experiments, the liquid bridges are formed of dimethylsiloxane with relevant material parameters surface tension $\gamma = 20.6$ mN/m and contact angle $\theta = 0^\circ$. The liquid bridge volume V has been varied, see Tab. (1).

Table 1: Input values for DEM-simulations of a single pair of particles with a liquid bridge between them, based on Willett's [27] and Rabinovich's [18] experiments

CODE	R_i [mm]	R_j [mm]	γ [mN/m]	θ [°]	V [nl]
W ₁₁	2.381	2.381	20.6	0	13.6
W ₁₂	2.381	2.381	20.6	0	31.3
W ₁₃	2.381	2.381	20.6	0	74.2
W ₂₁	2.381	1.588	20.6	0	9.6
W ₂₂	2.381	1.588	20.6	0	13.2
W ₂₃	2.381	1.588	20.6	0	24.7
W ₂₄	2.381	1.588	20.6	0	59.3
W ₃₁	2.381	1.191	20.6	0	25.3
W ₃₂	2.381	1.191	20.6	0	61.8
W ₃₃	2.381	1.191	20.6	0	127.8

	R_i [μm]	R_j [μm]	γ [mN/m]	θ [°]	V [$\times 10^8 \text{nm}^3$]
R ₁	19	35	27	10	2
R ₂	19	32.5	24	10	12
R ₃	19	27.5	28	10	36

Rabinovich et al. [18] used in their study much smaller glass spheres with the radii $R = [19 \dots 35] \mu\text{m}$. An oil with relevant material parameters $\gamma = [24 \dots 28] \text{mN/m}$ and $\theta = [0 \dots 10]^\circ$ forms the capillary bridges between the particles. All parameters for DEM-simulations are presented in Tab. (1).

Each of the 13 cases given in Tab. (1) was investigated in DEM simulations using the four CBMs of Weigert et al. (Weig), Willett et al. - full (WilF), Willett et al. - reduced (WilR) and Rabinovich et al. with Lambert's correction (RabL).

In the simulations, two interacting particles touch each other in their initial positions without a gap between them, i. e. $a = 0$. Then, one particle is pulled out whereas the other remains fixed, until the rupture distance of the liquid bridge a_{crit} is reached. During the simulation, the force F_{cap} of the capillary bridge is constantly recorded. Gravitation is not taken into account in the simulation.

In figures 2 and 3, results for the capillary force calculation in two different DEM simulations (simulations W₁₁ and R₁ from Tab. (1)) are compared with the corresponding experimental data. All simulations are performed until $a > a_{crit}$, therefore the jumps at the end of the curves represent the modeling of the liquid bridge rupture.

Obviously, the overall agreement of the CBMs WilF, WilR and RabL to both experimental data sets from the micro- and the nano-scale is very good (see insets on diagrams to get a zoomed view of the data). Differences between the CBMs predictions

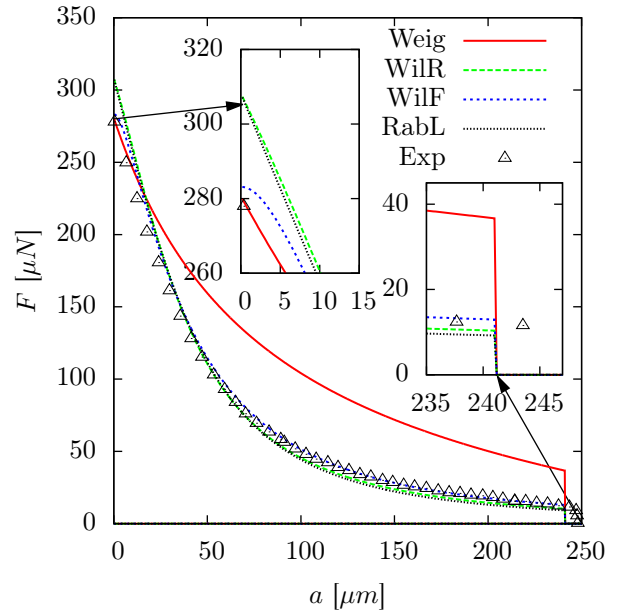


Figure 2: Capillary force as a function of separation distance, comparison of Willett experiments with simulations, [27, Fig. 1a, S. 9399], W₁₁, see Tab. (1): $R_i = R_j = 2.381 \text{ mm}$, $V = 13.6 \text{ nl}$

and measurements are largest for small particle distances a , i. e. small bridge elongations. It looks like this difference is not systematic, but random. Only in figure 2 Weig and WilF come close to experimental results for $a \rightarrow 0$; in figure 3 all CBMs fail to predict the measured values for F_{cap} in the case of $a \rightarrow 0$. We also have to keep in mind that measurements of capillary forces at such small separation distances are also complicated (see the discussion in [18]).

On the contrary, the DEM simulations with CBM Weig fit only for small values of a to the experimental findings. Especially for the micro-scale setup W₁₁ in figure 2, the CBM Weig is noticeably better in comparison to the other CBMs. However, the prediction quality of the Weig CBM rapidly decreases for moderate and large values of a . Only the qualitative trend (nonlinear decreasing capillary force with increasing a) is captured with CBM Weig, but the capillary force values are markedly over-predicted.

An overview over the results from all DEM simulations (setups W₁₁ ... W₃₃ and R₁ ... R₃) is given in figure 4. Here, relative capillary force values, defined as the ratio of numerical to experimental force data, are given for three different bridge lengths $a_1 = 0$, $a_2 = 0.5 a_{crit}$ and $a_3 = 0.95 a_{crit}$. In general, the observations from setups W₁₁ and R₁ are

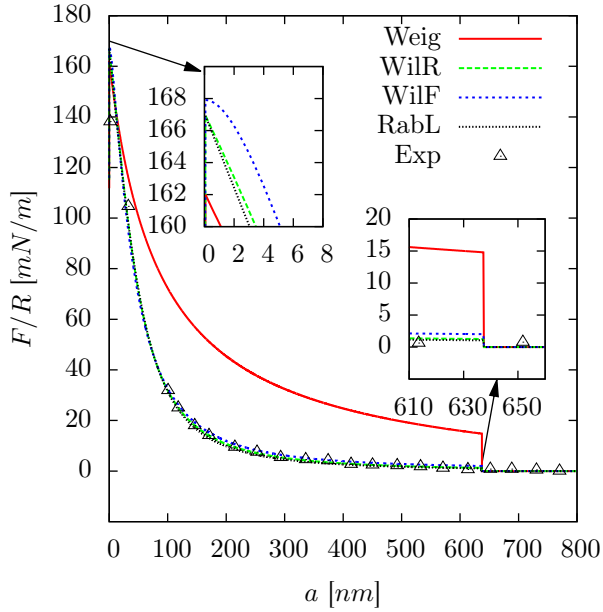


Figure 3: Capillary force as a function of separation distance, comparison of Rabinovich experiments with simulations, line 1, [18, Fig. 4, S. 10996], R_1 , see Tab. (1): $R_i = 19\mu\text{m}$, $R_j = 35\mu\text{m}$, $V = 2 \times 10^8 \text{ nm}^3$

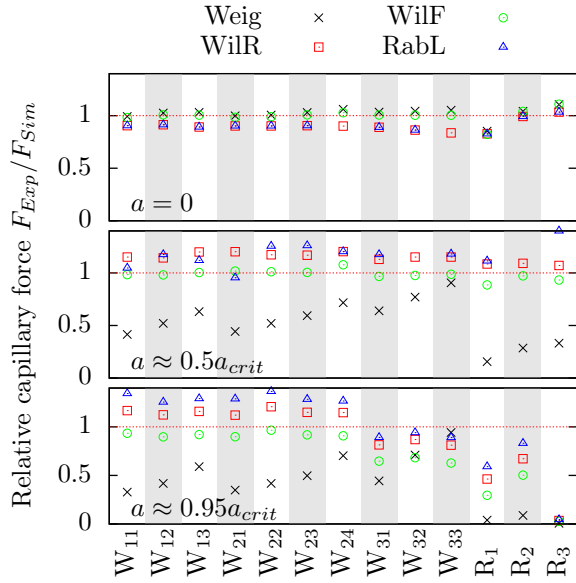


Figure 4: Capillary forces, obtained from simulations, are compared with experimental data (red dashed line)

confirmed: whereas CBMs WilF, WilR and RabL match well to the measurements for most setups

and all particle distances, the Weig CBM only gives only a satisfactory prediction for small a values.

4. Influence on macroscopic parameters

4.1. Shear cell setup

In a recent paper [24] the authors have demonstrated the visible influence of capillary forces on macroscopic hydrodynamic material parameters, e.g. “viscosity” (ratio of shear stress to strain rate), of wet granular matter in shearing motion. Now, the effects of the different CBMs on these parameters are studied. Therefore, DEM-simulations of a split-bottom ring-shear cell filled with a spherical beads are performed. The construction of such kind of ring-shear cell was proposed and experimentally examined by Fenistein et al. [1].

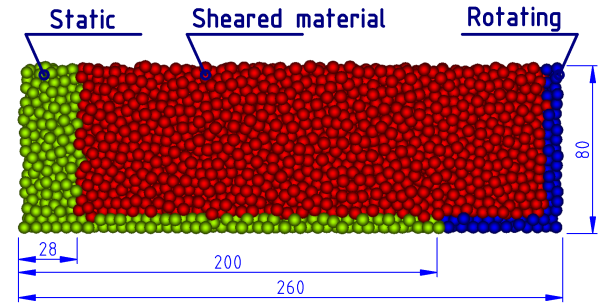


Figure 5: Setup of the split-bottom ring-shear cell in the DEM simulations. The center line of the rotational symmetrical geometry is on the left, radii and height are given in mm.

The geometry of the packing in the shear cell is given in figure 5. The particle size of the monodisperse packing has been set to $R_i = R_j = 2.381 \text{ mm}$, as in experiment W_{11} in Tab. (1). The outer cylinder and the outer part of the bottom of the shear cell rotates with a period of 100 s. The inner cylinder and the inner part of the bottom remain static.

The density of sheared particles is set to $\rho = 150 \text{ kg/m}^3$ in order to get roughly the same mass of particles as in [24] and achieve a comparable F_{norm}/F_{cap} relationship. The particle number for the simulation is nearly 200000. About 84% of all particles are in the region of the sheared material. The following model parameters are set: duration of contact $t_c = 5.4 \cdot 10^{-4} \text{ s}$, coefficient of restitution in normal and tangential directions $e_n = e_t = 0.83$, integration time step $\Delta t = 5.4 \cdot 10^{-4} \text{ s}$. Accord-

ing to formulation in [16] spring and damping coefficient under these conditions are the following: $k_n \approx 144.03$ N/m, $k_t \approx 41.15$ N/m, $c_n \approx 2.92 \cdot 10^{-3}$ kg/s and $c_t \approx 41.15$ kg/s. The Coulomb friction of the contact is set to $\mu = 0$ to exclude the influence of this parameter on the final results.

These settings of material parameters for the shear cell setup are purely artificial and do not correspond to any experiments. They have been chosen to see the effects of capillary bridges more clearly. Simulations with more realistic material parameters and comparison with data from shear cell experiments (not available at the moment) are planned for the future.

Liquid bridge volume values for simulations of weakly wetted material have been chosen to be 13.6 and 74.2 nl, which correspond to experiments of single pairs of particles W_{11} and W_{13} from Tab. (1) respectively. The distribution of capillary contacts is homogeneous without liquid conservation for the whole system. There are no interrelations between individual capillary bridges. Therefore, a slight fluctuation of up to 1% in the total liquid content was observed in the simulations.

Every simulation has been run for a minimum of 5 s real flow time, corresponding to $\approx 10^6$ simulation time steps. The potential and kinetic energies of all simulated particles were controlled. The results showed that such a low relatively simulation time is enough to achieve a steady state of the velocity field. This is in agreement with experimental studies of ring shear cell configurations [1, 2, 21]. However the whole system may also show some long-term transition in other quantities, e.g. density, which was recently shown by Sakaie et al. [21]. We do not consider these long-term developments, because we are focusing here on the velocity field analysis. The influence of the long-term behavior will be investigated for further studies.

All simulations have been carried out on the HPC cluster of TU Bergakademie Freiberg. Adding capillary bridges to the contact model of the DEM code increases the time of contact existence and the number of interactions. It complicates the calculation schema, but does not significantly decrease the calculation speed of the model. All simulations need nearly the same CPU time period with differences of only $\approx 10\%$. From every simulation, 15 snapshots are taken into account for averaging, see [24] for more details. The discrete averaging time step is 0.25 s.

4.2. Results and discussion

For the analysis, data obtained from DEM simulations was averaged by micro-macro transition as explained e.g. in [17, 24]. Therefore, all quanti-

ties, e.g. velocity, stress and strain presented in the section are macro-quantities.

The dominating feature in the sheared granular material in the split-bottom shear cell is the shear band, i.e. a localized region where the granular material yields and flows [1]. In figure 6, the shear bands in dry and wet granular materials are compared. For the wet materials, resulting shear bands from the four CBMs Weig, WilF, WilR and RabL are shown.

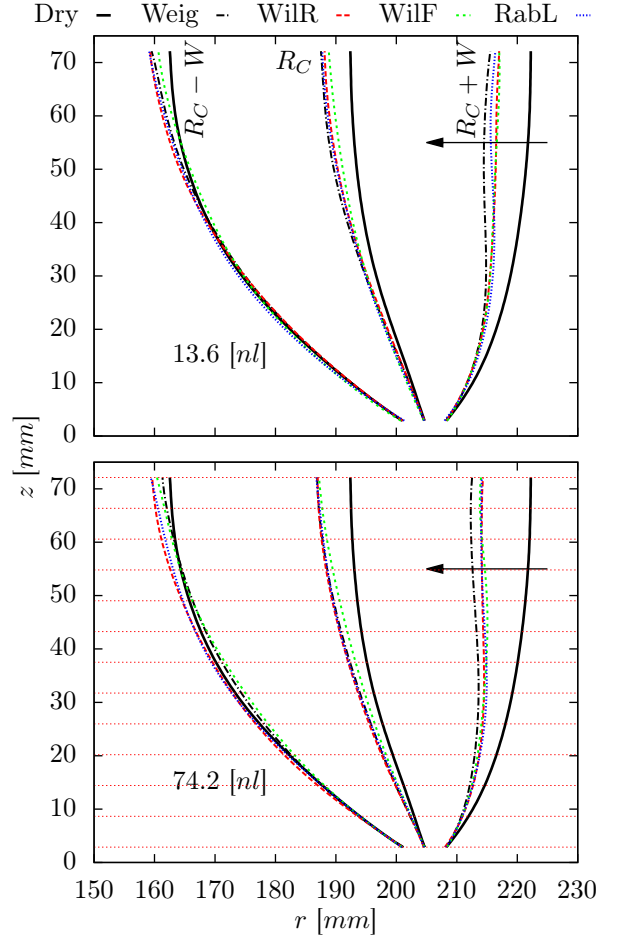


Figure 6: Shear bands and rates in dry (black thick line) and wet (dashed thin lines) materials. Lines indicate the centers R_C and widths W of shear bands, which were obtained through the fit of error function Eq. (13). Horizontal red lines on the lower plot are the heights at which the velocity profiles were analyzed.

Shear bands are indicated in figure 6 by lines. They were obtained through the fit of error function Eq. (13), which describes the universal velocity profile (see for details [1, 2, 17, 24]) of the sheared material. The central points of the shear band and its width were obtained for 13 different heights of

the sheared material

$$\omega(r) = 0.5 + 0.5 \cdot \operatorname{erf} \left(\frac{r - R_C}{W} \right) \quad (13)$$

where $\omega(r)$ is the velocity profile at the defined height of the layer, R_C and W are shear band center and width respectively.

Obviously, the center R_C and outer lines $R_C + W$ of the shear band are shifted inwards in the wet materials. The displacement seems to depend on the liquid content as well. For the larger liquid bridge volume (higher liquid content in the granular material), a stronger shift is observed. Regarding the four employed CBMs, we do not find a clear difference between the corresponding results (relocation of the shear bands). Similar shear band shifts were also observed by Luding during investigation of the friction influence on the sheared material [17].

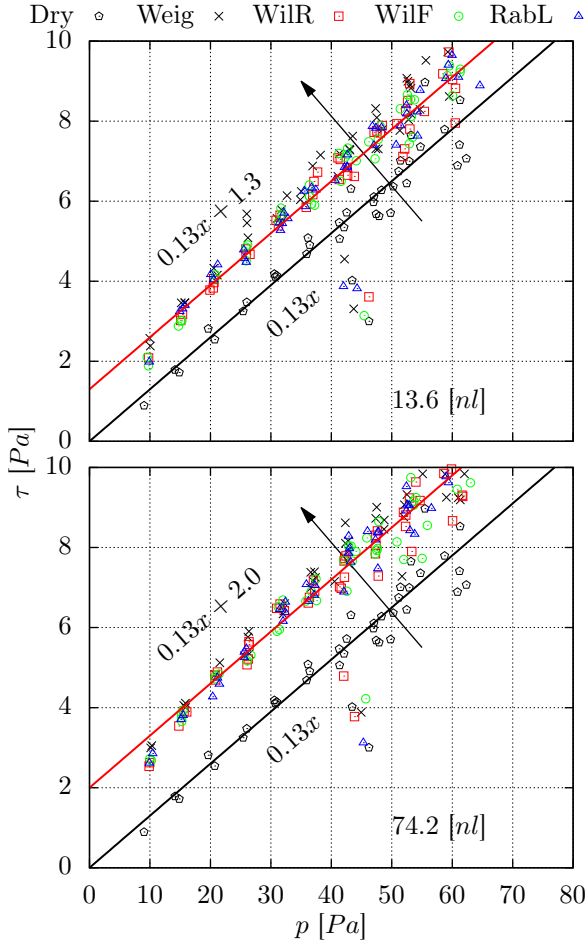


Figure 7: Shear stress τ plotted against pressure p where $\dot{\gamma} > 0.12$. Diagrams are showing the appeared cohesiveness of wet material.

The mean shear and normal stresses correlations τ - p give first insights into the macroscopic behavior

of the granular material in the shear band. Figure 7 shows these correlations for dry and wet material with different liquid content. As expected, the correlations fit to the well-known constitutive law [12]

$$\tau = \mu p + c \quad (14)$$

with $\mu = 0.13$ for the particular granular material. Here, the parameter c of the constitutive law depends significantly on the liquid content ($c_1 = 1.3 \text{ Pa}$ for $V_1 = 13.6 \text{ nl}$, $c_2 = 2 \text{ Pa}$ for $V_2 = 74.2 \text{ nl}$), whereas the choice of the CBM has again no obvious influence on the macroscopic parameters (all points fitted by the red lines are very close to each other). It is definitely seen that the liquid bridge existence and liquid content amount is increasing cohesiveness of the simulated media. The increase of the parameter c is due to the larger rupture distance a_{crit} , which is increasing proportionally to the liquid bridge volume. Therefore, the capillary forces act longer in the case of larger liquid bridge volumes. However the macro-correlations cannot be easily anticipated from the functional relationship given by the CBM. We have researched for such simple correlations between micro- and macro-scale functional relationships, but we have not found any at the moment.

The influence of the Coulomb friction parameter μ_C on shear band structure and parameter μ is the same as reported by Luding [17] for dry materials. Therefore a discussion is omitted here.

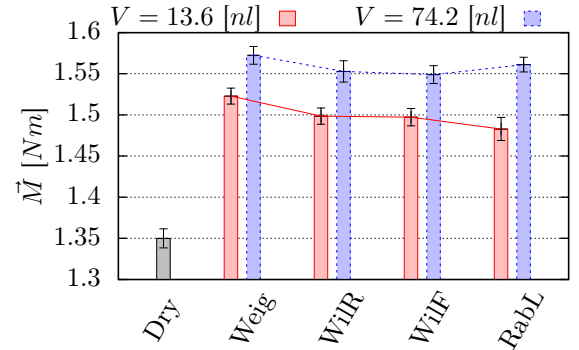


Figure 8: Average torque acting on rotating part of the shear cell during different simulation regimes.

One more macro-parameter, which can be evaluated from the DEM results, is the torque M acting on the rotating part of the shear cell. The torque indicates indirectly the cohesive properties of the sheared material as well. It has been recorded during the whole rotating period of the simulations. Time-averaged results are presented in figure 8. The results show the nonlinear dependency of the torque on the liquid content in the granular material, which can be the result of nonlinear CBM

dependency. Again, the DEM simulations with the four different CBMs give nearly the same values of M .

We conclude from the results in figures 6 to 8, that the specific choice of the CBM has a minor importance for this type of granular flow. Changes in the overall flow field structure and corresponding hydrodynamic parameters correlate clearly with the liquid content in the granular material, but only slightly with details of the capillary bridge force modelling.

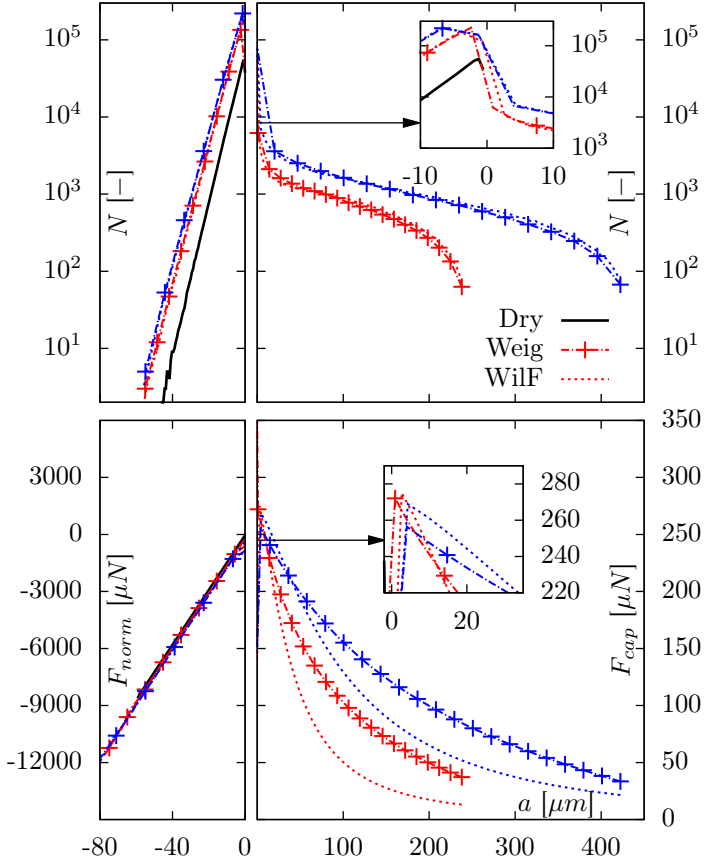


Figure 9: Contact number as a function of separation distance a (top row) for CBMs Weig and WilF. The bottom row shows the averaged force as a function of separation distance (right side) / penetration (left side) in a bulk. Blue lines – 74.2 [nl], red lines – 13.6 [nl]. (WilR and RabL are excluded from the diagram, it is difficult to distinguish them from WilF).

In order to understand these findings, we analyze the liquid bridge length distribution within the shear zone in more detail. Figure 9 gives the contact number and force distribution in both dry (mechan-

ical contact $a = -\delta_n$) and wet (bridge length $a > 0$) contacts respectively. The averaging is performed as given in Eq. (15)

$$\Phi(a) = \frac{1}{\Delta a} \int_{a-\Delta a/2}^{a+\Delta a/2} \phi(a) da \quad (15)$$

for the contact number N and the force F , respectively. The averaging interval is $\Delta a = (a_{crit} + \delta_{n,max})/100$, where $\delta_{n,max}$ is the maximum penetration distance of spheres found in the simulation. The inlay in the figure 9 (bottom row) shows, that the maximum of capillary force values is not exactly at $a = 0$ as can be seen in figure 2. That is an artifact due to the averaging interval, which is not present in simulation of an individual particle pair.

It is found that in the simulation of weakly wetted granular material, the number of mechanical contacts increases by about 20%, and is nearly independent of the individual liquid bridge volume. Inspecting the wet contacts, one can observe that most of them have only short bridge lengths with respect to a_{crit} . Here, the capillary force prediction gives roughly the same values from all four investigated CBMs. Therefore, only small deviations are found for the macroscopic flow parameters.

Also, the figure 9 (bottom row) shows distance-force dependencies, obtained from the shear cell simulations. Those curves have the same dependency as in the previous sphere-sphere simulations (figure 2). It proves the correct implementation of CBMs in the source code. Under the more dynamic conditions (increased cell rotation speed and thereby higher impact velocities), obtained curves can differ in a dry state from static ones because of the increased damping term of the total contact force.

Figure 10 shows the typical picture of wet contact distribution inside of the shear band and out of it. To correctly compare contact numbers, the wet contact number per volume n is introduced here. The diagram shows that the relative number of contacts varies only for the range $a > 0.5a_{crit}$.

The relative contact number is smaller for the range $a > 0.5a_{crit}$ outside the shear band compared to the region of the shear band itself. The trend is independent of liquid volume. In other words, in the shear band there are some more wet contacts, which are far away from each other due to the higher velocity gradient.

5. Conclusion

In the paper, four different capillary bridge models for DEM simulations are investigated. First,

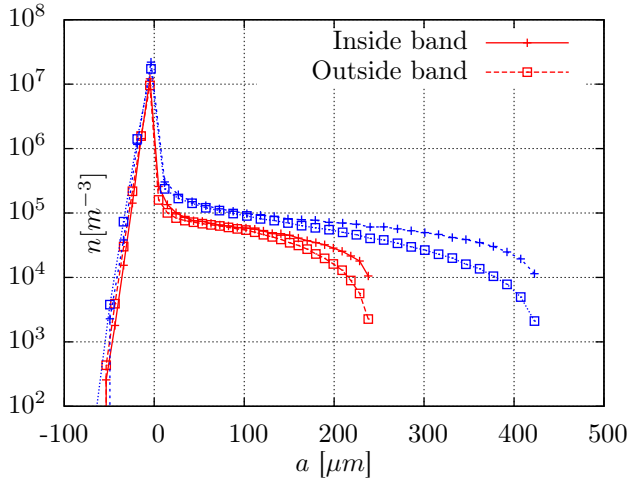


Figure 10: Contact density as a function of separation distance a inside shear band and outside of it for RabL CBM. Blue symbols – 74.2 [nl], red lines – 13.6 [nl]

implementations of the four capillary bridge models in DEM are validated by a comparison of simulation results and experimental measurements of an individual micro-scale pendular bridge between two separating spheres. It is found that the results of three capillary bridge models are very near to the experimental data. In contrast, one model only gives a reasonable qualitative representation of the capillary force development, but overestimates the force values strongly.

Then, the different capillary bridge models are employed in DEM simulations of wet granular material sheared in a split-bottom shear cell. Here, the flow field structure and corresponding macroscopic parameters clearly depend on the micro-scale parameter liquid bridge volume. However, up to now, the investigated macroscopic rheological dependencies of the sheared material cannot be easily anticipated from the functional microscopic relationships given by the CBM.

Additionally, the differences that have been found in the prediction of individual bridges on the micro-scale are not visible on the macro-scale in this specific configuration. Therefore, the specific choice of the investigated capillary bridge model does not seem to have a marked influence on the prediction of the hydrodynamics of this type of granular flow. Separation distance a for most of the wet contacts in the bulk is relatively small in comparison to the critical distance a_{crit} , where all CBMs showed comparable results.

Disclosure

The authors express their thanks to the Deutsche Forschungsgemeinschaft, which supported this work within the DFG/STW project SCHW 1168/6-1 “Hydrodynamic theory of wet particle systems”.

Acknowledgments

Special thanks go to Stefan Luding and our partners at TU Dortmund and UTwente in this project for the helpful discussion.

The final publication is available at www.springerlink.com

References

- [1] FENISTEIN, D., VAN DE MEENT, J. W., AND VAN HECKE, M. Universal and wide shear zones in granular bulk flow. *Phys. Rev. Lett.* 92 (Mar 2004), 094301.
- [2] FENISTEIN, D., VAN DE MEENT, J. W., AND VAN HECKE, M. Core precession and Global Modes in Granular Bulk Flow. *Phys. Rev. Lett.* 96 (2006), 118001.
- [3] GABRIELI, F., LAMBERT, P., COLA, S., AND CALVETTI, F. Micromechanical modelling of erosion due to evaporation in a partially wet granular slope. *International journal for numerical and analytical methods in geomechanics* 36, 7 (2012), 918–943.
- [4] GAN, Y., MAGGI, F., BUSCARNERA, G., AND EINAV, I. A particle-water based model for water retention hysteresis. *arXiv preprint arXiv:1307.5372* (2013).
- [5] HERMINGHAUS, S. Dynamics of wet granular matter. *Advances in Physics* 54, 3 (2005), 221–261.
- [6] IVESON, S. M., LITSTER, J. D., HAPGOOD, K., AND ENNIS, B. J. Nucleation, growth and breakage phenomena in agitated wet granulation processes: a review. *Powder Technology* 117, 1 (2001), 3–39.
- [7] LAMBERT, P. *Capillary forces in microassembly: modeling, simulation, experiments, and case study*. Springer, 2007.
- [8] LAMBERT, P., CHAU, A., DELCHAMBRE, A., AND RÉGNIER, S. Comparison between two capillary forces models. *Langmuir* 24, 7 (2008), 3157–3163.

- [9] LAMBERT, P., AND REGNIER, S. Surface and contact forces models within the framework of microassembly. *Journal of Micromechanics* 3, 2 (2004), 123–158.
- [10] LIAN, G., THORNTON, C., AND ADAMS, M. J. A theoretical study of the liquid bridge forces between two rigid spherical bodies. *Journal of Colloid and Interface Science* 161, 1 (1993), 138–147.
- [11] LIU, P., YANG, R., AND YU, A. Dynamics of wet particles in rotating drums: Effect of liquid surface tension. *Physics of Fluids* 23 (2011), 013304.
- [12] LUDING, S., AND ALONSO-MARROQUÍN, F. The critical-state yield stress (termination locus) of adhesive powders from a single numerical experiment. *Granular Matter* 13, 2 (2011), 109–119.
- [13] MANI, R., KADAU, D., AND HERRMANN, H. J. Liquid migration in sheared unsaturated granular media. *Granular Matter* 15, 4 (2013), 447–454.
- [14] MITARAI, N., AND NORI, F. Wet granular materials. *Advances in Physics* 55, 1-2 (2006), 1–45.
- [15] PIETSCH, W., AND RUMPF, H. Haftkraft, kapillardruck, flüssigkeitsvolumen und grenzwinkel einer flüssigkeitsbrücke zwischen zwei kugeln. *Chemie Ingenieur Technik* 39, 15 (1967), 885–893.
- [16] POURNIN, L., LIEBLING, T. M., AND MOCELLIN, A. Molecular-dynamics force models for better control of energy dissipation in numerical simulations of dense granular media. *Phys. Rev. E* 65, 1 (Dec 2001), 011302.
- [17] PROF.DR. S. LUDING. The effect of friction on wide shear bands. *Particulate science and technology* 26, 1 (2008), 33–42.
- [18] RABINOVICH, Y. I., ESAYANUR, M. S., AND MOUDGIL, B. M. Capillary forces between two spheres with a fixed volume liquid bridge : Theory and experiment. *Langmuir* 21, 24 (2005), 10992–10997. eng.
- [19] RADJAI, F., AND DUBOIS, F. *Discrete-Element Modeling of Granular Materials*. John Wiley & Sons, 2011.
- [20] RADL, S., KALVODA, E., GLASSER, B. J., AND KHINAST, J. G. Mixing characteristics of wet granular matter in a bladed mixer. *Powder Technology* 200, 3 (2010), 171–189.
- [21] SAKAIE, K., FENISTEIN, D., CARROLL, T. J., VAN HECKE, M., AND UMBANHOWAR, P. Mr imaging of reynolds dilatancy in the bulk of smooth granular flows. *EPL (Europhysics Letters)* 84, 3 (2008), 38001.
- [22] SCHOLTÈS, L., HICHER, P.-Y., NICOT, F., CHAREYRE, B., AND DARVE, F. On the capillary stress tensor in wet granular materials. *International journal for numerical and analytical methods in geomechanics* 33, 10 (2009), 1289–1313.
- [23] SCHWAGER, T., AND PÖSCHEL, T. Coefficient of restitution and linear-dashpot model revisited. *Granular Matter* 9, 6 (2007), 465–469.
- [24] SCHWARZE, R., GLADKY, A., UHLIG, F., AND LUDING, S. Rheology of weakly wetted granular materials: a comparison of experimental and numerical data. *Granular Matter* 15, 4 (2013), 455–465.
- [25] SOULIE, F., CHERBLANC, F., EL YOUSOUFI, M. S., AND SAIX, C. Influence of liquid bridges on the mechanical behaviour of polydisperse granular materials. *International journal for numerical and analytical methods in geomechanics* 30, 3 (2006), 213–228.
- [26] WEIGERT, T., AND RIPPERGER, S. Calculation of the liquid bridge volume and bulk saturation from the half-filling angle. *Particle & Particle Systems Characterization* 16, 5 (1999), 238–242.
- [27] WILLETT, C. D., ADAMS, M. J., JOHNSON, S. A., AND SEVILLE, J. P. K. Capillary bridges between two spherical bodies. *Langmuir* 16, 24 (2000), 9396–9405.
- [28] ZHU, H., ZHOU, Z., YANG, R., AND YU, A. Discrete particle simulation of particulate systems: theoretical developments. *Chemical Engineering Science* 62, 13 (2007), 3378–3396.
- [29] ŠMILAUER, V., CATALANO, E., CHAREYRE, B., DOROFEENKO, S., DURIEZ, J., GLADKY, A., KOZICKI, J., MODENESE, C., SCHOLTÈS, L., SIBILLE, L., STRÁNSKÝ, J., AND THOENI, K. *Yade Documentation*, 1st ed. The Yade Project, 2010. <http://yade-dem.org/doc/>.

A. Weigert’s model equations

The following equations are used for the calculation of β , C_a and C_θ , p_k , R_1 and R_2 for Weigert’s model. V (bridge volume) can be found as:

$$V = 0.12(2R)^3 \sin^4 \beta C_a C_\theta \quad (\text{A1})$$

Since V is a given parameter for us, β can be obtained:

$$\beta = \arcsin \left(\frac{V}{0.12 \cdot (2R)^3 \cdot C_a C_\theta} \right)^{1/4} \quad (\text{A2})$$

C_a and C_θ are the correction functions for the distance and the contact angles respectively, they are calculated according to:

$$C_a = \left(1 + 6 \frac{a}{2R} \right) \quad (\text{A3})$$

$$C_\theta = (1 + 1.1 \cdot \sin \theta) \quad (\text{A4})$$

The capillary pressure p_k is calculated according to the Laplace-Young equation:

$$p_k = \gamma \left(\frac{1}{R_1} + \frac{1}{R_2} \right) \quad (\text{A5})$$

The principal radii of the bridge curvature R_1 and R_2 are taken positive and negative respectively, and calculated according to Pietsch and Rumpf [15]:

$$R_1 = \frac{R(1 - \cos \beta) + a}{\cos(\beta + \theta)} \quad (\text{A6})$$

$$R_2 = R \sin \beta + R_1 [\sin(\beta + \theta) - 1] \quad (\text{A7})$$

The full description of the model can be found here [26].

B. Willett's full model equations

The coefficients $f_{1...4}$ of Willett's full model are calculated as follows:

$$\begin{aligned} f_1 = & (-0.44507 + 0.050832 \theta - 1.1466 \theta^2) + \\ & (-0.1119 - 0.000411 \theta - 0.1490 \theta^2) \ln(V^*) + \\ & (-0.012101 - 0.0036456 \theta - 0.01255 \theta^2) (\ln(V^*))^2 + \\ & (-0.0005 - 0.0003505 \theta - 0.00029076 \theta^2) (\ln(V^*))^3; \end{aligned} \quad (\text{B1})$$

$$\begin{aligned} f_2 = & (1.9222 - 0.57473 \theta - 1.2918 \theta^2) + \\ & (-0.0668 - 0.1201 \theta - 0.22574 \theta^2) \ln(V^*) + \\ & (-0.0013375 - 0.0068988 \theta - 0.01137 \theta^2) (\ln(V^*))^2 \end{aligned} \quad (\text{B2})$$

$$\begin{aligned} f_3 = & (1.268 - 0.01396 \theta - 0.23566 \theta^2) + \\ & (0.198 + 0.092 \theta - 0.06418 \theta^2) \ln(V^*) + \\ & (0.02232 + 0.02238 \theta - 0.009853 \theta^2) (\ln(V^*))^2 + \\ & (0.0008585 + 0.001318 \theta - 0.00053 \theta^2) (\ln(V^*))^3; \end{aligned} \quad (\text{B3})$$

$$\begin{aligned} f_4 = & (-0.010703 + 0.073776 \theta - 0.34742 \theta^2) + \\ & (0.03345 + 0.04543 \theta - 0.09056 \theta^2) \ln(V^*) + \\ & (0.0018574 + 0.004456 \theta - 0.006257 \theta^2) (\ln(V^*))^2; \end{aligned} \quad (\text{B4})$$

The full description of the model can be found here [27].